# Identifying Four Obesity Axes Through Integrative Multiomics and Imaging Analysis

Chiemela S. Odoemelam,[1] Afreen Naz,[1] Marjola Thanaj,[2] Elena P. Sorokin,[3] Brandon Whitcher,[2] Naveed Sattar,[4] Jimmy D. Bell,[2] E. Louise Thomas,[2] Madeleine Cule,[3] and Hanieh Yaghootkar[1]

*Diabetes 2025;74:1168–1183 | https://doi.org/10.2337/db24-1103*

**We aimed to identify distinct axes of obesity using advanced magnetic resonance imaging (MRI)–derived phenotypes. We used 24 MRI-derived fat distribution and muscle volume measures (UK Biobank; *N* = 33,122) to construct obesity axes through principal component analysis. Genome-wide association studies were performed for each axis to uncover genetic factors, followed by pathway enrichment, genetic correlation, and Mendelian randomization analyses to investigate disease associations. Four primary obesity axes were identified: *1*) general obesity, reflecting higher fat accumulation in all regions (visceral, subcutaneous, and ectopic fat); *2*) muscle dominant, indicating greater muscle volume; *3*) peripheral fat, associated with higher subcutaneous fat in abdominal and thigh regions; and *4*) lower-body fat, characterized by increased lower-body subcutaneous fat and reduced ectopic fat. Each axis was associated with distinct genetic loci and pathways. For instance, the lower-body fat axis was associated with *RSPO3* and *COBLL1*, which are emerging as promising candidates for therapeutic targeting. Disease risks varied across axes; the general obesity axis was correlated with higher risks of metabolic and cardiovascular diseases, whereas the lower-body fat axis seemed to protect against type 2 diabetes and cardiovascular disease. This study highlights the heterogeneity of obesity through the identification of obesity axes and emphasizes the potential to extend beyond BMI in defining and treating obesity for obesity-related disease management.**

### ARTICLE HIGHLIGHTS

- This study aimed to address potential limitations of BMI by exploring the heterogeneity of obesity using magnetic resonance imaging–derived fat distribution and muscle volume measures.
- We sought to identify distinct obesity axes and investigate their genetic, metabolic, and disease associations.
- Four obesity axes were identified (general obesity, muscle dominant, peripheral fat, and lower-body fat), each linked to unique genetic loci, metabolic traits, and disease risks.
- These findings emphasize the potential to extend beyond BMI in defining and managing obesity, offering a more nuanced framework for understanding and treating obesity-related diseases.

Obesity presents with a range of metabolic patterns, disease risks, and responses to weight loss interventions among individuals (1–4). This variability is largely due to the traditional clinical definition of obesity, which uses a BMI threshold of $>30$ kg/m$^2$ to identify at-risk groups (1). Although this measurement effectively categorizes obesity at the population level, it fails to capture the heterogeneity among individuals (5). This broad metric, although useful for public health strategies, is inadequate for the nuanced requirements of precision medicine that necessitate tailored approaches.

Numerous studies have explored the complexities of obesity by identifying specific subtypes, notably focusing on metabolically healthy obesity, where individuals exhibit no initial

[1]School of Natural Science, College of Health and Science, University of Lincoln, Lincoln, U.K.
[2]Research Center for Optimal Health, School of Life Sciences, University of Westminster, London, U.K.
[3]Calico Life Sciences, LLC, South San Francisco, CA
[4]School of Cardiovascular and Metabolic Health, University of Glasgow, Glasgow, U.K.

Corresponding author: Hanieh Yaghootkar, hyaghootkar@lincoln.ac.uk

Received 3 December 2024 and accepted 22 April 2025

This article contains supplementary material online at https://doi.org/10.2337/figshare.28839827.

C.S.O. and A.N. contributed equally to this work.

metabolic dysfunctions despite living with obesity (6). However, the stability of this state is uncertain, because many may develop metabolic complications over time as they gain weight or age (2,6). The use of biomarkers to classify obesity into subtypes and guide personalized treatments has been proposed (2,7). However, gathering biomarker data postdiagnosis can challenge causal interpretations because of potential reverse causation, where the disease itself might influence biomarker levels (8). Additionally, the reliance on BMI hinders these methods, because it fails to differentiate between fat and muscle mass or consider the importance of fat distribution (1,2). These limitations mean that even those within a normal BMI range can face metabolic challenges, whereas some individuals with obesity might display metabolic resilience (2,9).

Recent advancements in magnetic resonance imaging (MRI) technology and the availability of comprehensive scan data from participants in UK Biobank have opened new avenues for detailed assessments of fat and muscle across various body regions. These image-derived phenotypes (IDPs) enable the classification of obesity axes without preconceived hypotheses by examining diverse fat distribution patterns in subcutaneous and ectopic locations.

In this study, we used 24 MRI-derived fat distribution and muscle measurements to agnostically construct four principal component (PC)–derived obesity axes. These axes are linear combinations of the IDPs, representing distinct dimensions of obesity, and allow us to move beyond traditional BMI classifications. We demonstrate that these axes capture unique patterns of fat distribution and muscle volume that are linked to different genetic profiles and disease risks. By integrating advanced imaging with genetic analysis, this study offers a comprehensive framework to better understand obesity heterogeneity, paving the way potentially for more targeted approaches in obesity management and treatment.

## RESEARCH DESIGN AND METHODS

### Study Design

We applied 24 MRI-derived measures of fat distribution (volumes and percentages) and muscle indices from UK Biobank to construct obesity axes. Analyses were conducted separately for men and women because of known sex-specific differences in fat distribution patterns. After confirming consistent PC patterns across sexes, we performed meta-analyses of genome-wide association study (GWAS) results for each axis. We investigated genetic correlations with metabolic biomarkers, lifestyle, behavior, and psychological disorders. Additionally, we performed Mendelian randomization (MR) to explore relationships between each axis and obesity-related disease risks.

### Image-Derived Measures of Fat Distribution and Muscle Volume

We used neck-to-knee Dixon MRI and single-slice multiecho MRI acquisitions for abdominal imaging, as previously outlined in the UK Biobank protocol (10). Image processing was conducted using deep learning models, as previously described (11–14). The IDPs included volume and median proton density fat fraction, calculated via the phase regularized estimation using the smoothing and constrained optimization method (15). Quality control was performed by analyzing univariate distributions and visually inspecting scans for anomalies.

Supplementary Table 1 details the 24 IDPs used in this study, including subcutaneous adipose tissue volumes (abdominal and thigh), visceral adipose tissue volumes, internal fat and thigh intermuscular adipose tissue volumes (corrected for muscle volume), and iliopsoas and total muscle volumes (indexed to height$^2$). We also obtained a measure of fat (proton density fat fraction) stored in the liver, pancreas, and paraspinal muscles (intramyocellular fat) from the single-slice multiecho acquisition.

### Construction of Obesity Axes

PC analysis (PCA) was applied to the 24 IDPs to identify obesity axes. PCA, a robust and widely validated dimensionality reduction technique, captures dominant patterns of variation across data sets while minimizing noise. Each IDP was scaled and standardized to mean zero and unit variance. Resultant PCs were oriented to align with higher obesity levels. The number of PCs retained was determined based on the proportion of variance explained (>85% cumulatively) and the interpretability of the components.

Given sex-specific differences in fat and muscle distribution, PCA was conducted separately for men and women. Meta-analysis was subsequently performed on follow-up analyses (e.g., GWAS) for consistent axes across sexes, ensuring that male PC1 aligned with female PC1, male PC2 with female PC2, and so forth.

We did not include BMI or total body fat percentage as a covariate in our analyses because these measures are highly correlated with certain axes, particularly the general obesity and muscle-dominant axes. Adjusting for these variables could obscure the meaningful variation in fat distribution and muscle composition that our MRI-derived phenotypes capture.

### GWAS

Using REGENIE (version 3.1.1) (16), which is well suited for association testing in the presence of closely related individuals, our GWAS included participants who self-identified as White British who clustered with this group in PCA. We excluded participants with sex chromosome anomalies, sex discrepancies, heterozygosity outliers, and genotype call rate outliers (17). Covariates included age, squared age, genotyping array, imaging center, and the first 10 genotype-related PCs. Imputed single nucleotide polymorphisms, filtered by a minor allele frequency >0.01 and an INFO score >0.9, resulted in 9,788,243 single nucleotide polymorphisms for the final analysis. GWAS was conducted separately for each sex,

followed by a meta-analysis using METAL to integrate results across sexes.

### Pathway and Tissue Enrichment Analysis

We used the SNP2GENE function in the Functional Mapping and Annotation (18) platform to identify expression quantitative trait loci (eQTLs) using the GTEx (version 8) project (19). Identified genes were analyzed for pathway enrichment using the PANTHER (version 17.0) tool (20), enhancing our understanding of the biological pathways enriched in our gene sets.

### Genetic Correlation Analysis

We estimated genetic correlations between obesity axes and various biomarkers, lifestyle traits, and psychological conditions using LD score regression (21). We selected 110 traits using publicly available GWAS summary statistics (Supplementary Table 2) based on established links with obesity and body composition. It is important to note that some of these GWAS included UK Biobank participants. Although incorporating these data sets increases our statistical power, it may also introduce a degree of sample overlap, potentially inflating genetic correlation estimates. We set a multiple testing–corrected significance level at $P < 0.05/110 * 4 = 0.00011$.

### MR

To investigate the potential causal impacts of different obesity axes on disease outcomes, we applied MR (Supplementary Table 2). Genetic variants were selected as instrumental variables for each obesity axis based on stringent criteria: $P \leq 5 \times 10^{-8}$ and linkage disequilibrium pruning with $r^2 > 0.001$ within a 10-Mb window, using European ancestry data from the 1000 Genomes Project.

Our primary method was the inverse variance weighted (IVW) method. This method is subject to biases such as weak instrument bias, where the weak association between genetic instruments and exposures can skew estimates, and horizontal pleiotropy, where genetic variants may influence outcomes through pathways unrelated to the studied exposure. To try to counteract these potential biases, we confirmed strong associations between each genetic instrument and its corresponding obesity axis ($F$ statistics >10) and used MR-Egger regression to test for horizontal pleiotropy, as indicated by the Egger intercept. Additionally, we applied methods like MR-PRESSO, weighted median, simple mode, and weighted mode to enhance the robustness of our findings (22). We adjusted the results for multiple testing using Benjamini-Hochberg correction and considered results statistically significant at an adjusted $P$ value <0.05.

### Data and Resource Availability

Our research was conducted using UK Biobank data. Under the standard UK Biobank data sharing agreement, we (and other researchers) cannot directly share raw data obtained or derived from UK Biobank. However, under this agreement, all of the data generated and methodologies used in this study are returned by us to UK Biobank, where they will be fully available. Access can be obtained directly from UK Biobank to all bona fide researchers on submitting a health-related research proposal to UK Biobank at https://www.ukbiobank.ac.uk.

## RESULTS

### Axes of Obesity

In our study, we analyzed data from 33,122 participants who underwent MRI scanning in the UK Biobank study. We derived 24 IDPs from these samples, with sample characteristics detailed in Supplementary Table 1. Using these IDPs, we constructed four obesity axes through PCA performed separately for men and women. Each measure was oriented to positively correlate with BMI. The resulting obesity axes explained 4.43% to 57.50% of the variance in men and 5.89% to 54.76% in women (Supplementary Figs. 1 and 2). Consistent PC patterns across sexes allowed us to meta-analyze results for equivalent PCs (e.g., male PC1 with female PC1) (Fig. 1 and Supplementary Table 3).

We named the axes based on their PC loadings (Fig. 1): *1*) general obesity axis, which reflects increased fat accumulation across all regions, including visceral, subcutaneous, and ectopic fat (Fig. 2*A* and *B*); *2*) muscle-dominant axis, which indicates greater muscle volume (Fig. 2*C* and *D*); *3*) peripheral fat axis, which is associated with higher subcutaneous fat in the abdominal and thigh regions (Fig. 2*E* and *F*); and *4*) lower-body fat axis, which is characterized by increased lower-body subcutaneous fat and reduced ectopic fat in the liver, pancreas, and muscles (Fig. 2*G* and *H*).

To better contextualize the axes within clinical obesity definitions, we examined the BMI distributions of individuals in the top 10% of each axis (Supplementary Table 4). Individuals in the top 10% of all axes showed significantly higher BMI ($P < 0.0001$), with most having a BMI >30 kg/m$^2$, suggesting that high scores on these axes generally reflect a phenotype consistent with clinical obesity. However, the observed differences between axes indicate that even among individuals classified as having obesity by BMI criteria, there is substantial heterogeneity in fat distribution.

Axes represent overlapping dimensions rather than discrete categories. Muscle-dominant and peripheral fat axes displayed a weak negative correlation, suggesting that individuals scoring high on one axis tend to score lower on the other (Supplementary Fig. 3).

### Relationship Between Axes and Age

We analyzed the relationship between PC scores and age for all obesity axes in men and women. Scores for the general obesity axis increased with age ($r_{men} = 0.15$ and $P_{men} < 1E{-}10$; $r_{women} = 0.10$ and $P_{women} < 1E{-}10$), indicating a higher likelihood of accumulating fat in older individuals. Conversely, scores for the muscle-dominant ($r_{men} = -0.48$ and $P_{men} < 1E{-}10$; $r_{women} = -0.36$ and $P_{women} < 1E{-}10$), peripheral fat ($r_{men} = -0.14$ and $P_{men} < 1E{-}10$; $r_{women} = -0.10$

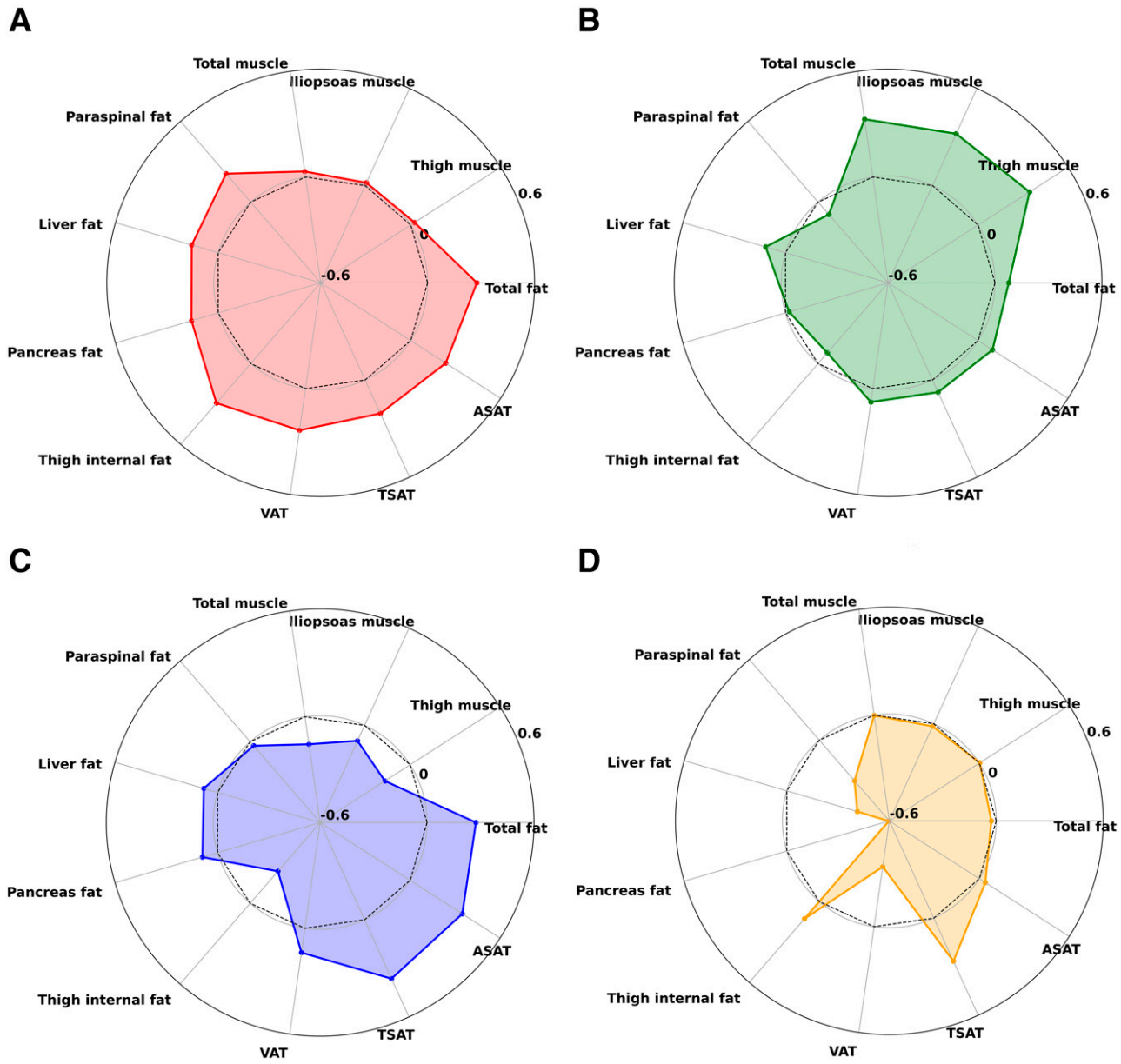


**Figure 1—**Characteristics of obesity axes. Radial plots display the magnitudes of PC loadings for the four obesity axes from men (*A–D*) and women (*E–H*). Points above the inner circle indicate positive loadings, reflecting traits that contribute positively to the respective obesity axis, whereas points below the inner circle represent negative loadings, indicating traits that contribute inversely to the axis. General obesity (*A* and *E*), muscle dominant (*B* and *F*), peripheral fat (*C* and *G*), and lower-body fat (*D* and *H*) axes are shown. ASAT, abdominal subcutaneous adipose tissue; TSAT, thigh subcutaneous adipose tissue; VAT, visceral adipose tissue.

and $P_{\text{women}} < 1E{-}10$), and lower body fat ($r_{\text{men}} = -0.18$ and $P_{\text{men}} < 1E{-}10$; $r_{\text{women}} = -0.24$ and $P_{\text{women}} < 1E{-}10$) axes decreased with age, suggesting these patterns of fat or muscle distribution are less common among older individuals (Fig. 3).

### Differences in Axes by Ancestry

To explore potential differences in the distribution of obesity axes across ancestry groups, we categorized participants into four major genetic ancestry groups: African ancestry ($n$ = 146), Central/South Asian ancestry ($n$ = 320), East Asian ancestry ($n$ = 152), and European ancestry ($n$ = 29,179). Comparisons revealed that East Asian individuals had lower scores for the general obesity ($P_{\text{EUR vs. EAS}} < 0.00001$) and lower-body fat axes ($P_{\text{EUR vs. EAS}} < 0.00004$). Central/South Asian individuals had lower scores for the muscle-dominant axis ($P_{\text{EUR vs. CSA}} < 0.00001$), whereas individuals of African ancestry had higher scores for the muscle-dominant and lower-body fat axes but lower scores for the peripheral fat axis (all $P_{\text{EUR vs. AFR}} < 0.00001$) (Fig. 4 and Supplementary Table 5).

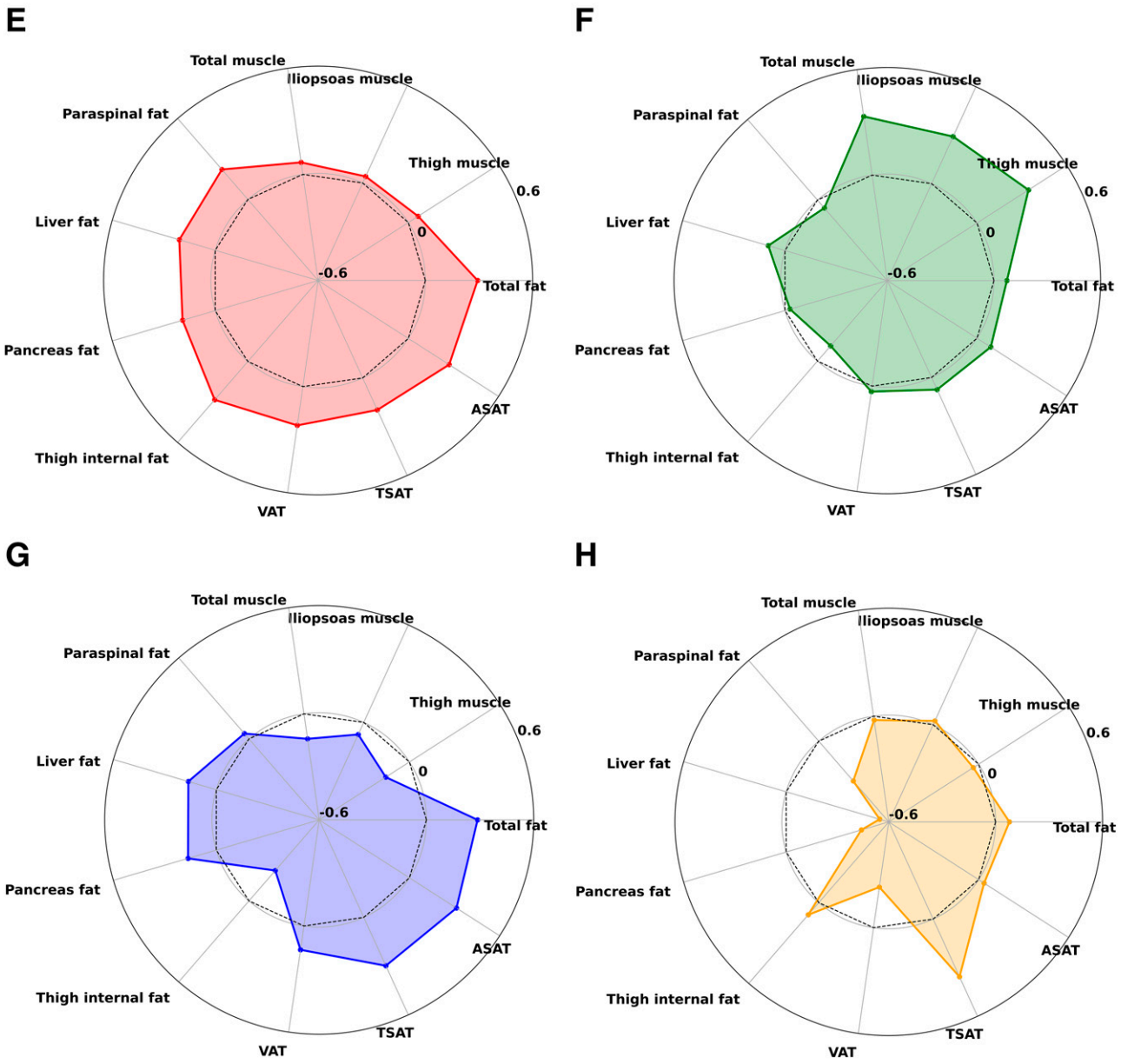


**Figure 1**—Continued

## Genetic Background of Obesity Axes

Given the ancestry-related differences in axis distribution, and to minimize confounding from unrelated factors (e.g., β-cell function differences influencing type 2 diabetes risk in individuals of African ancestry), all genetic analyses were restricted to White British participants. GWAS were conducted separately for men and women and meta-analyzed across sexes for consistent axes, resulting in a total sample size of 25,637 (Table 1 and Supplementary Figs. 4 and 5). No evidence of sex-specific associations was observed, because the genetic loci contributing to the axes were consistent between men and women (Supplementary Table 6).

### *General Obesity Axis*

Two significant loci were identified: rs62033405 (eQTL for *FTO* in skeletal muscle; $P$ = 2.6E−7 and *IRX1* in pancreas; $P$ = 1.2E−7) and rs33823 (eQTL for *PEPD* in skeletal muscle; $P$ = 4.9E−9 and subcutaneous adipose tissue; $P$ = 5E−6), both previously associated with obesity-related traits. Pathway enrichment highlighted the corticosteroid receptor signaling pathway; however, these results did not remain significant after Bonferroni correction (Supplementary Table 7).

### *Muscle-Dominant Axis*

Nine loci were associated, including rs7515497 near *FBLIM1*, rs80345488 near *RIMS2* (eQTL for *RIMS2* in

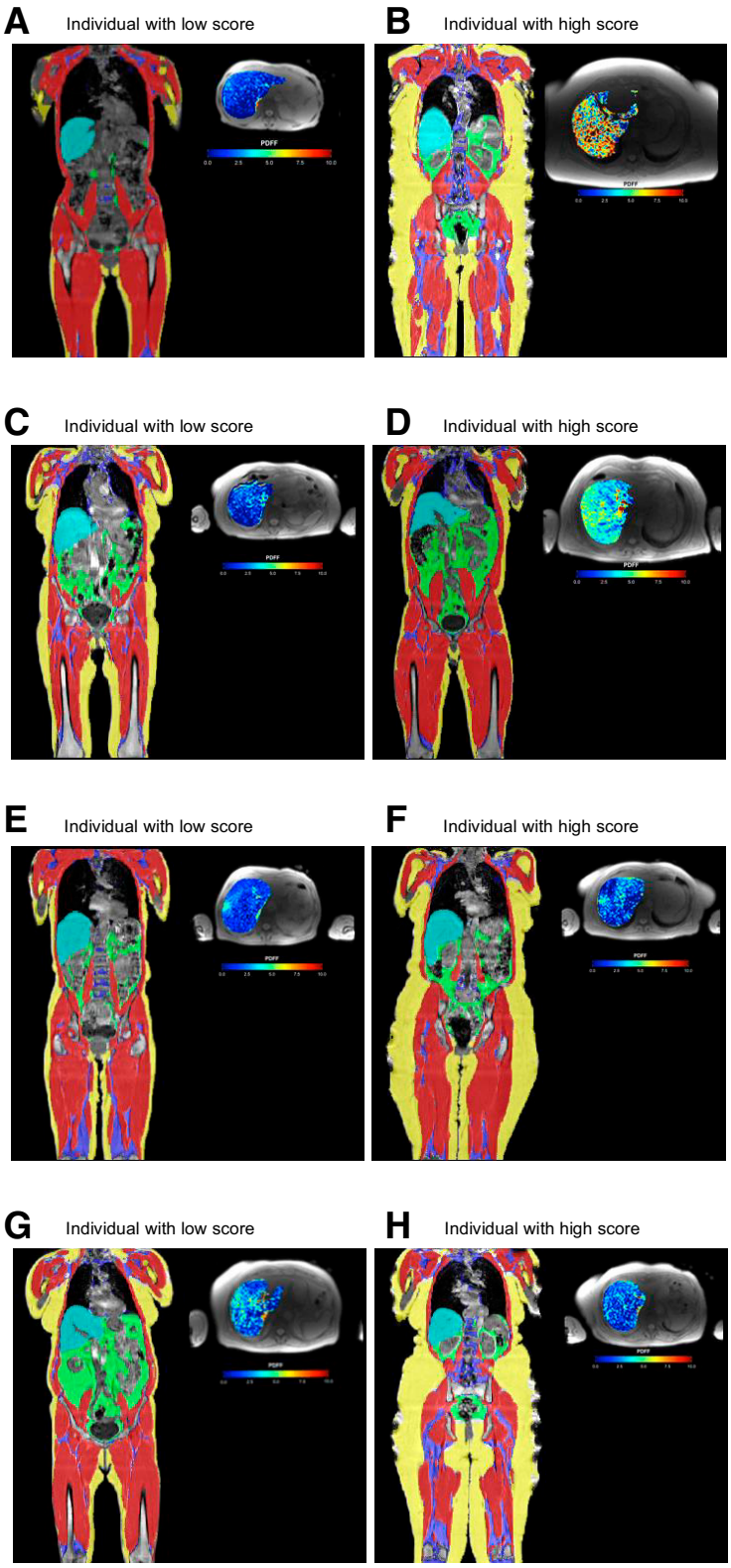


**Figure 2—**MRI scans and fat distribution patterns across obesity axes: general obesity (*A* and *B*), muscle dominant (*C* and *D*), peripheral fat (*E* and *F*), and lower-body fat (*G* and *H*). MRI scans illustrate the contrasting fat distribution patterns observed in individuals with the lowest (*A*, *C*, *E*, and *G*) and highest (*B*, *D*, *F*, and *H*) scores along each obesity axis. These visual comparisons highlight the distinctive anatomical fat accumulation and muscle distribution associated with each axis.

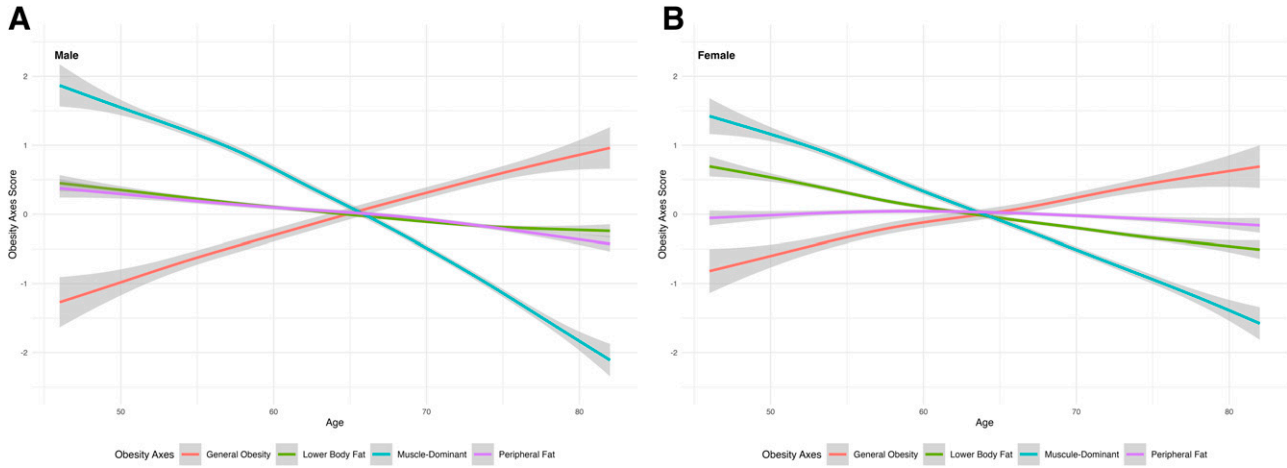


**Figure 3—**Relationship between obesity axes and age in men (*A*) and women (*B*). Scatter plots depict the variation in scores for each obesity axis across different ages. General obesity scores tended to increase with age, whereas scores for other axes, such as the lower-body fat axis, decreased in older individuals.

thyroid; $P$ = 7E−18), rs3850625, an exonic variant in *CACNA1S*, rs12632536 (eQTL for *DLG1* in skeletal muscle; $P$ = 1.2E−7), rs13170533 (splicing QTL for *PIK3R1* in skeletal muscle; $P$ = 2.2E−6), rs1028883 (eQTL for *KLF5* in skeletal muscle; $P$ = 6.6E−38), rs6058093 near *PIGU* (eQTL for *GGT7*; $P$ = 1E−6 and *MAP1LC3A*; $P$ = 8E−9 in skeletal muscle), and rs9306468 near *MTMR3* (eQTL for *THOC5* in skeletal muscle; $P$ = 2E−8). Pathway enrichment analysis revealed nominally significant enrichment in pathways related to muscle function, particularly ion transport, muscle contraction, and structural integrity; however, these results did not remain significant after Bonferroni correction (Supplementary Table 8).

### *Peripheral Fat Axis*

Fifteen loci were identified, many of which have been previously linked to waist-to-hip ratio (WHR), lipid levels, type 2 diabetes, or red blood cell count. Three loci were shared between the peripheral and lower-body fat axes, including *COBLL1*, *RSPO3*, and *DNAH10/CCDC92* (Supplementary Fig. 6). Pathway enrichment analysis for the peripheral fat axis revealed several key pathways. These include pathways related to cellular growth and energy metabolism, which may affect adipocyte behavior, and mechanisms that regulate cell-matrix interactions and developmental processes influencing fat distribution; however, these results did not remain significant after Bonferroni correction (Supplementary Table 9).

### *Lower-Body Fat Axis*

Fifteen loci were identified, including rs1128249 (splicing QTL for *COBLL1* in subcutaneous fat; $P$ = 5E−13), rs72959041 (eQTL for *RSPO3* in subcutaneous fat; $P$ = 2E−8 and protein QTL [pQTL] in blood; $P$ = 6E−89), rs7133378 near *DNAH10* (eQTL for *DNAH10OS* in subcutaneous fat; $P$ = 1E−32), rs3818717 near *RAI1* (eQTL for *TOM1L2* in subcutaneous fat; $P$ = 1E−15 and pQTL for *SHMT1*; $P$ = 1E−42), rs6822892 (eQTL for *PDGFC* in subcutaneous fat; $P$ = 3E−8), rs10406327 (eQTL for *PEPD* in subcutaneous fat; $P$ = 1E−11), rs2287922, an exonic variant in *RASIP1*, rs3747207 near *PNPLA3* (eQTL for *SAMM50* in subcutaneous fat; $P$ = 7E−15), rs2943653 near *NYAP2* (eQTL for *IRS1* in subcutaneous fat; $P$ = 2E−13), rs6888037 near *SLC12A2*, rs998584 near *VEGFA*, rs12138803 near *PIGC*, rs55893113 near *ZC3H11B*, rs754243 near *ANAPC1*, and rs58542926 near *TM6SF2* (pQTL for NCAN; $P$ = 4E−92 and SUGP1; $P$ = 6E−12). Pathway enrichment analysis indicated a significant potential role of adiponectin in metabolic regulation and the importance of lipid biosynthesis processes in maintaining healthier adipose tissue; however, these results did not remain significant after Bonferroni correction (Supplementary Table 10).

## Association With Metabolic Biomarkers

We performed LD score regression to evaluate the genetic correlations between obesity axes and a wide range of complex traits, including anthropometric measures, metabolic biomarkers, lifestyle behaviors, psychological traits, and obesity-related diseases. Of 110 traits tested, 53 showed significant genetic correlations (corrected for multiple testing) with at least one obesity axis.

All obesity axes demonstrated positive genetic correlations with adult BMI. The general obesity axis showed strong positive correlations with body fat percentage, WHR in both sexes, and childhood obesity. The muscle-dominant axis correlated positively with fat-free mass index, height, birth weight, and childhood obesity. The peripheral fat axis was positively correlated with body fat percentage and WHR in men. In contrast, the lower-body fat axis was negatively correlated with WHR in both sexes but positively associated with birth weight and childhood obesity (Fig. 5*A*).

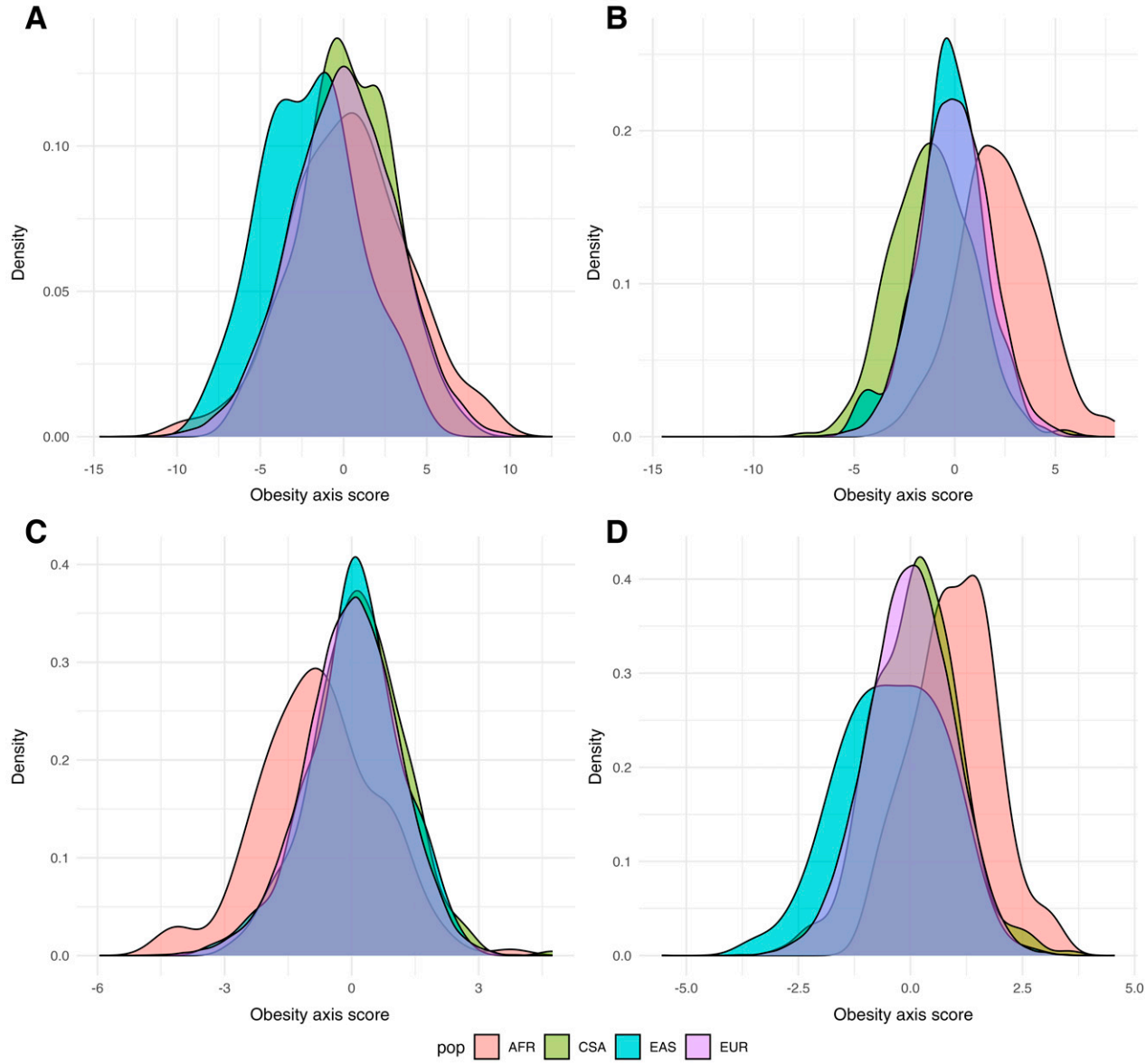


**Figure 4**—Ancestry-related variation in obesity axes: general obesity (*A*), muscle dominant (*B*), peripheral fat (*C*), and lower-body fat (*D*). Density plots show the distribution of scores for each obesity axis across different ancestry groups: African (AFR), Central/South Asian (CSA), East Asian (EAS), and European (EUR). pop, population.

Each obesity axis had a distinct pattern of genetic correlation with metabolic traits and health outcomes (Fig. 5*B*). The general obesity axis showed positive correlations with insulin resistance markers, C-reactive protein, liver enzymes, branched-chain amino acids (valine, leucine, and isoleucine), and triglycerides, while demonstrating negative correlations with sex hormone–binding globulin, HDL cholesterol (HDL-C), and apolipoprotein A1. The muscle-dominant axis did not present extensive correlations but showed a strong positive association with HOMA for insulin resistance and a negative correlation with HDL-C. The peripheral fat axis correlated positively with fasting insulin and C-reactive protein levels. In contrast, the lower-body fat axis was positively associated with insulin sensitivity, sex hormone–binding globulin, and HDL-C and negatively associated with branched-chain amino acids and triglycerides.

Additionally, the general obesity axis was positively correlated with sedentary behavior, smoking, attention-deficit/hyperactivity disorder, substance use, and binge eating. Conversely, the muscle-dominant axis was negatively correlated with sleep duration, whereas the peripheral fat axis was negatively correlated with physical activity (Fig. 5*C*). These findings underscore the complex and distinct metabolic and lifestyle associations for each obesity axis.

### Association With Disease Outcomes

In our UK Biobank imaging subcohort, the general obesity axis was associated with a higher risk of various

**Table 1—Genetic results for different obesity axes**

| Obesity axis | rsID | Chr | Position | *P* | EA | NEA | β | SE | Nearest gene | Parameter(s) previously associated with locus |
|---|---|---|---|---|---|---|---|---|---|---|
| General obesity | rs62033405 | 16 | 53822387 | 5.6E−11 | T | C | 0.06 | 0.01 | *FTO* | Obesity, metabolic traits |
| | rs33823 | 19 | 34000725 | 8.2E−10 | T | C | 0.06 | 0.01 | *PEPD* | Obesity, metabolic traits |
| Muscle dominant | rs7515497 | 1 | 16120240 | 2.6E−8 | T | G | −0.04 | 0.01 | *FBLIM1* | — |
| | rs3850625 | 1 | 201016296 | 4.5E−8 | A | G | −0.07 | 0.01 | *CACNA1S* | Lean mass, creatinine, estimated glomerular filtration rate, lung function, liver enzymes |
| | rs2138157 | 2 | 227103717 | 1.4E−8 | A | C | −0.05 | 0.01 | *IRS1* | Lipids, obesity, other metabolic biomarkers |
| | rs12632536 | 3 | 196833650 | 4E−9 | T | C | −0.05 | 0.01 | *DLG1* | Lung function, creatinine, estimated glomerular filtration rate |
| | rs13170533 | 5 | 68058041 | 4.6E−9 | C | G | −0.08 | 0.01 | *SLC30A5* | Creatinine levels, estimated glomerular filtration rate, lung function |
| | rs80345488 | 8 | 104536643 | 4.7E−8 | A | C | 0.10 | 0.02 | *RIMS2* | — |
| | rs1028883 | 13 | 74108587 | 4.2E−9 | T | G | −0.05 | 0.01 | *KLF5* | Lean mass, liver enzyme levels, kidney function |
| | rs6058093 | 20 | 33213196 | 3.2E−10 | A | C | 0.05 | 0.01 | *PIGU* | Estimated glomerular filtration rate, liver enzymes, creatinine levels, lung function |
| | rs9306468 | 22 | 30374281 | 4.7E−9 | T | C | 0.05 | 0.01 | *MTMR3* | Lung function, estimated glomerular filtration rate, creatinine levels |
| Peripheral fat | rs11205797 | 1 | 51474198 | 2.9E−9 | A | G | −0.05 | 0.01 | *CDKN2C* | Red blood cell count |
| | rs566596164 | 2 | 165558215 | 4.2E−12 | C | G | 0.09 | 0.01 | *COBLL1* | WHR, lipids, type 2 diabetes, other metabolic biomarkers |
| | rs13172689 | 5 | 53463520 | 3.2E−10 | A | G | −0.07 | 0.01 | *ARL15* | Type 2 diabetes |
| | rs1651274 | 5 | 158020425 | 3.3E−8 | A | G | −0.06 | 0.01 | *EBF1* | WHR, lipids, type 2 diabetes, other metabolic biomarkers |
| | rs141783576 | 6 | 127439897 | 4.5E−12 | C | G | −0.12 | 0.02 | *RSPO3* | WHR, lipids, type 2 diabetes, other metabolic biomarkers |
| | rs10827616 | 10 | 36469937 | 1E−9 | T | C | 0.05 | 0.01 | *FZD8* | Red blood cell count |
| | rs7129492 | 11 | 74381181 | 2.1E−12 | A | G | −0.06 | 0.01 | *POLD3* | Colorectal cancer, creatinine |
| | rs11045236 | 12 | 20578939 | 3E−9 | T | C | −0.06 | 0.01 | *PDE3A* | White blood cell count, lipids, $HbA_{1c}$ |
| | rs11057413 | 12 | 124489162 | 2.9E−9 | A | G | −0.05 | 0.01 | *ZNF664*, *FAM101A* | WHR, lipids, type 2 diabetes, other metabolic biomarkers |
| | rs749170 | 13 | 22350875 | 3.3E−10 | T | C | −0.06 | 0.01 | *FGF9* | Platelet count, SHBG, liver enzyme |
| | rs3116602 | 13 | 51111355 | 5.1E−12 | T | G | −0.07 | 0.01 | *DLEU1* | WHR, lipids |
| | rs9565581 | 13 | 81098500 | 2.5E−13 | A | C | −0.07 | 0.01 | *SPRY2* | Body fat |
| | rs1883711 | 20 | 39179822 | 1.5E−9 | C | G | −0.15 | 0.02 | *SNORD112* | Lipids, metabolic biomarkers |

*Continued on p. 1177*

**Table 1—Continued**

| Obesity axis | rsID | Chr | Position | *P* | EA | NEA | β | SE | Nearest gene | Parameter(s) previously associated with locus |
|---|---|---|---|---|---|---|---|---|---|---|
| | rs11698277 | 20 | 45502865 | 5.3E−14 | T | C | −0.07 | 0.01 | *EYA2* | WHR |
| | rs2267373 | 22 | 38600542 | 1.9E−12 | T | C | −0.06 | 0.01 | *PLA2G6*, *MAFF* | WHR, lipids, type 2 diabetes, other metabolic biomarkers |
| Lower-body fat | rs12138803 | 1 | 172348823 | 3.1E−8 | T | C | −0.05 | 0.01 | *DNM3*, *PIGC* | WHR, SHBG |
| | rs55893113 | 1 | 219773122 | 8E−9 | C | G | 0.05 | 0.01 | *ZC3H11B* | WHR, SHBG, lipids, type 2 diabetes |
| | rs754243 | 2 | 112251121 | 7.1E−10 | A | G | 0.06 | 0.01 | *ANAPC1* | WHR, SHBG |
| | rs1128249 | 2 | 165528624 | 1.1E−17 | T | G | 0.07 | 0.01 | *COBLL1* | Lipids, obesity, type 2 diabetes, other metabolic biomarkers |
| | rs2943653 | 2 | 227047771 | 1.1E−9 | T | C | −0.05 | 0.01 | *NYAP2* | Lipids, type 2 diabetes, metabolic biomarkers |
| | rs6822892 | 4 | 157734675 | 2.3E−8 | A | G | −0.05 | 0.01 | *PDGFC* | Lipids, type 2 diabetes, metabolic biomarkers |
| | rs6888037 | 5 | 127406259 | 2.2E−8 | T | G | −0.05 | 0.01 | *SLC12A2* | Lipids, measures of obesity, metabolic biomarkers |
| | rs998584 | 6 | 43757896 | 2.1E−18 | A | C | −0.07 | 0.01 | *VEGFA* | WHR, lipids, type 2 diabetes, metabolic biomarkers |
| | rs72959041 | 6 | 127454893 | 5.6E−11 | A | G | −0.13 | 0.02 | *RSPO3* | WHR, lipids |
| | rs7133378 | 12 | 124409502 | 1.6E−11 | A | G | 0.06 | 0.01 | *DNAH10*, *CCDC92* | WHR, lipids, type 2 diabetes |
| | rs3818717 | 17 | 17707105 | 1.3E−8 | T | C | −0.05 | 0.01 | *RAI1* | WHR, lipids, type 2 diabetes |
| | rs58542926 | 19 | 19379549 | 3.5E−19 | T | C | −0.14 | 0.02 | *TM6SF2* | Lipids, type 2 diabetes |
| | rs10406327 | 19 | 33890838 | 5.9E−9 | C | G | 0.05 | 0.01 | *PEPD* | WHR, type 2 diabetes |
| | rs2287922 | 19 | 49232226 | 2.3E−8 | A | G | −0.05 | 0.01 | *RASIP1* | WHR, lipids, other metabolic biomarkers |
| | rs3747207 | 22 | 44324855 | 3.5E−30 | A | G | −0.12 | 0.01 | *PNPLA3* | Liver enzymes, fatty liver, lipids, type 2 diabetes |

Chr, chromosome; EA, effect allele; NEA, noneffect allele; SHBG, sex hormone–binding globulin.

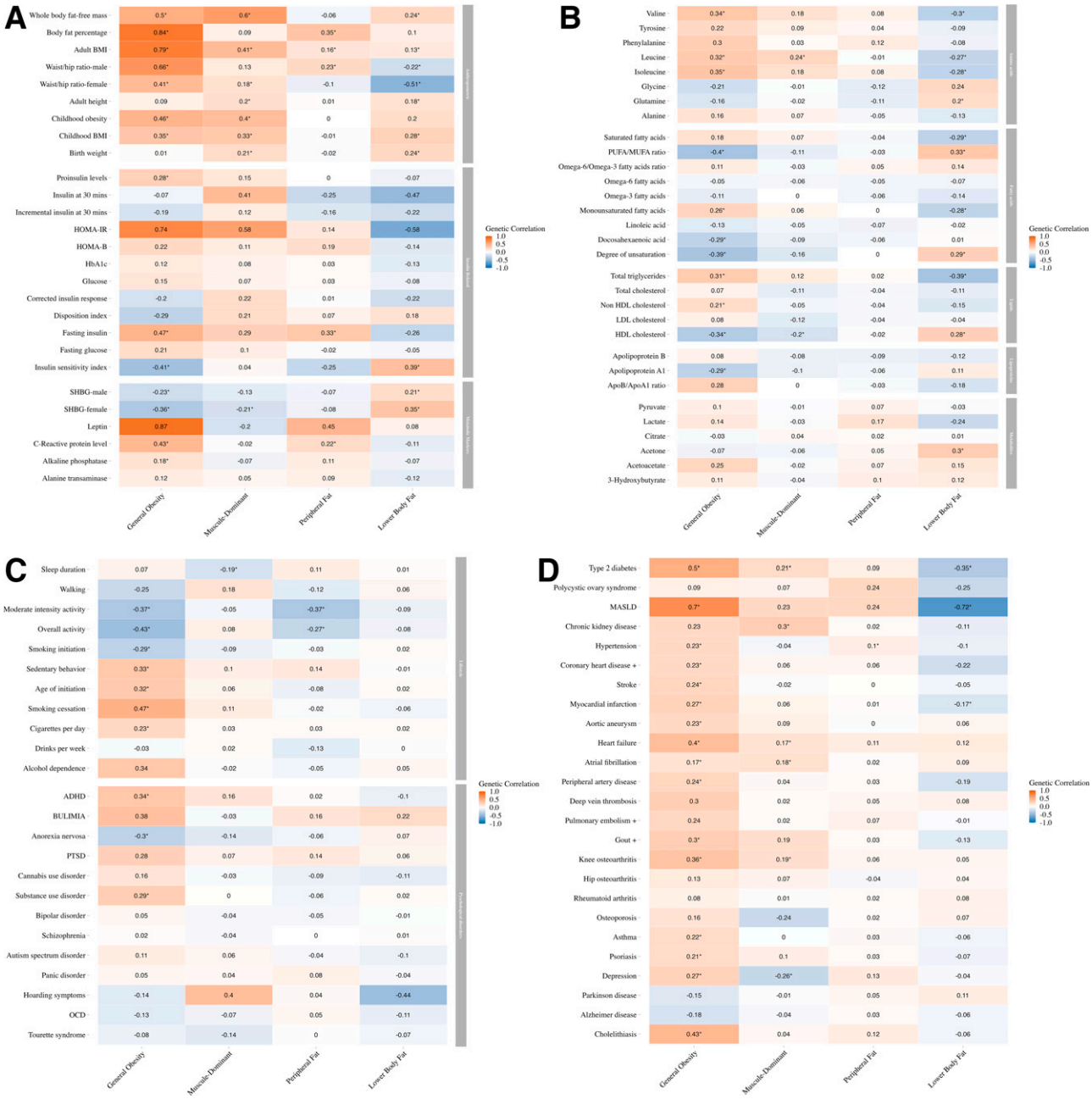


**Figure 5—**Genetic correlations between obesity axes and selected biomarkers, lifestyle traits, and psychological disorders. Heat map of genetic correlations (rg) between obesity axes and anthropometric traits, insulin-related traits, and metabolic biomarkers (*A*); metabolites (*B*); lifestyle traits and psychological disorders (*C*); and various disease outcomes, including cardiovascular disease and type 2 diabetes (*D*). Colors and their intensities represent the correlation coefficients (rg), with asterisks indicating statistical significance after multiple testing correction ($P < 0.00011$). ADHD, attention-deficit/hyperactivity disorder; HOMA-B, HOMA for β-cell function; HOMA-IR, HOMA for insulin resistance; MASLD, metabolic dysfunction–associated steatotic liver disease; MUFA, monounsaturated fatty acid; OCD, obsessive-compulsive disorder; PTSD, posttraumatic stress disorder; PUFA, polyunsaturated fatty acid; SHBG, sex hormone–binding globulin.

cardiovascular diseases, asthma, psoriasis, and depression but a lower risk of osteoporosis. In contrast, the lower-body fat axis was associated with a lower risk of cardiovascular diseases. For example, participants in the top 10% of the general obesity axis, as determined by their PC scores, had ∼25% (95% CI 22%–29%) higher odds of developing type 2 diabetes compared with those in the bottom 10% based on prevalent disease cases. Conversely, individuals in the top 10% of the lower-body fat axis had 55% lower odds (95% CI 50%–60%) of developing type 2 diabetes compared with those in the bottom 10% (Supplementary Fig. 7).

To validate these findings in studies independent of the UK Biobank data set, we performed genetic correlation


**Figure 6—**MR. The heat map illustrates causal associations between obesity axes and selected disease outcomes. Colors and their intensities represent the direction and strength of associations determined by the IVW method. Asterisks indicate statistical significance after Benjamini-Hochberg correction (adjusted $P < 0.05$). MASLD, metabolic dysfunction–associated steatotic liver disease.

analyses between the obesity axes and disease risks. The general obesity axis was genetically correlated with a higher risk of type 2 diabetes, steatotic liver disease, hypertension, coronary heart disease, stroke, myocardial infarction, aortic aneurysm, heart failure, peripheral artery disease, gout, osteoarthritis, asthma, psoriasis, depression, and cholelithiasis. The muscle-dominant axis was linked to a higher risk of type 2 diabetes, chronic kidney disease, atrial fibrillation, and osteoarthritis but a lower risk of depression. The peripheral fat axis did not present significant genetic correlations with major diseases. The lower-body fat axis was associated with a lower risk of type 2 diabetes, steatotic liver disease, and myocardial infarction (Fig. 5*D*).

MR analyses, using genetic instruments with robust *F* statistics ($F = 36$ for general obesity axis; $F = 31$ for muscle-dominant axis; $F = 42$ for peripheral fat axis; $F = 40$ for lower-body fat axis), provided support for causal associations between obesity axes and various disease outcomes (Fig. 6 and Supplementary Table 11). The general obesity axis was instrumented with only two variants, and

therefore, sensitivity tests such as MR-Egger could not be reliably performed; our conclusions for this axis are based solely on IVW estimates, which linked it to increased risks of osteoarthritis, asthma, cholelithiasis, and gastroesophageal reflux disease. For the muscle-dominant axis, although IVW indicated an increased risk of chronic kidney disease and osteoarthritis, the association with hip osteoarthritis was not replicated in the MR-Egger analysis. For the peripheral fat axis, sensitivity tests were generally consistent, except that MR-Egger did not confirm the association with chronic kidney disease, steatotic liver disease, or polycystic ovary syndrome. Finally, for the lower-body fat axis, a majority of MR sensitivity tests corroborated IVW findings, linking this axis to lower risks of type 2 diabetes, polycystic ovary syndrome, steatotic liver disease, hypertension, myocardial infarction, aortic aneurysm, and psoriasis and a higher risk of osteoarthritis; however, MR-Egger estimates failed to replicate associations for aortic aneurysm and coronary heart disease.

## DISCUSSION

This study presents a comprehensive exploration of obesity, leveraging advanced imaging and genetic analyses to unravel the complex pathways underlying obesity. Using MRI-derived phenotypes from UK Biobank, we identified four distinct axes of obesity: general obesity, muscle dominant, peripheral fat, and lower-body fat. These findings highlight the heterogeneity of obesity and underscore some limitations of conventional metrics like BMI in capturing the nuances of individual obesity-related risks and outcomes.

### Implications of Axes for Disease Risk

The identification of these axes provides important insights into disease mechanisms. The general obesity axis, characterized by overall fat accumulation, was strongly associated with increased risks of several metabolic and cardiovascular conditions, including type 2 diabetes, hypertension, myocardial infarction, and liver disease. These findings align with prior research linking overall adiposity to metabolic dysregulation and inflammation (23,24). Pathway enrichment analyses suggest a role for corticosteroid receptor signaling, although the extent of its direct contribution remains uncertain. Although elevated cortisol levels, as seen in conditions like Cushing's syndrome (25), are clearly implicated in metabolic disturbances, other factors likely play a more prominent role in general obesity.

The muscle-dominant axis, defined by increased muscle volume, presented a unique metabolic profile. Although higher HOMA for insulin resistance levels were observed, there was no association with other insulin sensitivity indices, suggesting insulin resistance might be confined to specific tissues such as the liver. The increased risks of chronic kidney disease and atrial fibrillation, coupled with a lower risk of depression, highlight the complexity of this axis. Previous studies have shown that increased muscle mass can have both beneficial and detrimental metabolic effects, depending on factors such as muscle composition and lipid infiltration (14,26). The elevated risks of chronic kidney disease and atrial fibrillation might indicate a link between greater muscle mass and increased cardiac workload, as well as renal strain resulting from increased protein metabolism and creatinine turnover. The lower risk of depression associated with this axis supports previous findings that greater muscle mass may be protective against mood disorders, potentially through improved physical function and self-perception (27). Genetic loci associated with the muscle-dominant axis, including *CACNA1S*, *DLG1*, and *PIK3R1*, further point to the importance of muscle function, ion transport, and insulin signaling in this phenotype.

The peripheral fat axis, associated with higher subcutaneous fat in the abdomen and thighs, demonstrated a relatively benign metabolic profile, with no significant genetic correlation with major disease outcomes. This finding aligns with previous studies indicating that subcutaneous fat, particularly in peripheral regions, is less metabolically detrimental than visceral fat (28–31). This contrasts with the general obesity axis, highlighting that not all forms of fat accumulation carry the same health risks.

The lower-body fat axis, marked by increased lower-body subcutaneous fat and reduced ectopic fat, exhibited a favorable metabolic profile. Participants with higher scores along this axis showed lower risks of type 2 diabetes, myocardial infarction, and fatty liver disease. These findings support the protective metabolic effects of gluteofemoral fat as a so-called safe storage depot, consistent with previous genetic studies (24,30,32,33). Pathway enrichment analyses highlighted the importance of adiponectin secretion and lipid biosynthesis, suggesting enhanced adipocyte function and fat storage capacity may drive this protective effect.

### Ancestry-Related Differences and Precision Medicine

Significant ancestry-related variations in the distribution of these axes were observed. For example, East Asian participants had lower scores for the general and lower-body fat axes, whereas African participants exhibited higher scores for the muscle-dominant and lower-body fat axes but lower scores for the peripheral fat axis. These differences underscore the need for ancestry-informed approaches in managing obesity and its associated disease risks. The metabolic risks tied to each axis may vary across populations, emphasizing the importance of moving beyond a one-size-fits-all strategy in obesity management (9,34).

### Genetic Insights

The GWAS identified distinct genetic loci and pathways associated with each axis, providing novel insights into the biological mechanisms underlying fat distribution patterns. For the muscle-dominant axis, several genes of particular interest were identified. *CACNA1S* has been linked to mild human myopathy, with supporting evidence from zebrafish models (35). Disruptions in *DLG1*, which impair

myosin distribution, can affect muscle efficiency and metabolic regulation (36). *PIK3R1* is critical in muscle metabolism, as demonstrated by knockout mice that resist glucocorticoid-induced insulin resistance and muscle atrophy, maintaining healthier muscle structure (37). *KLF5*, a zinc-finger transcription factor, is essential for cell proliferation and muscle regeneration (38). *GGT7* plays a key role in glutathione metabolism, protecting against oxidative stress and supporting muscle health (39). *MAP1LC3A* is involved in the autophagy pathway essential for muscle repair (40). *THOC5* influences muscle differentiation and hematopoiesis (41).

Genes highlighted for lower-body fat axis have been previously shown to be involved in adipose tissue function. Knocking down *COBLL1* disrupts fat storage by impairing stress fiber breakdown in subcutaneous fat cells, affecting insulin responsiveness and lipid metabolism (42). Variants in *RSPO3* suppress adipogenesis, promote apoptosis of gluteal adipocytes, limit adipose tissue expansion, and stimulate upper-body fat distribution (43). *DNAH10OS* regulates nearby genes like *DNAH10* and *CCDC92*, both involved in lipid accumulation in adipocyte models (30). SHMT2 deficiency in mice increases fatty liver, highlighting its role in fat metabolism (44). *PDGFC* regulates adipose tissue in response to dietary changes (45). *PEPD* is vital for collagen turnover in adipose tissue, with lower expression linked to increased fibrosis and insulin resistance (46). *RASIP1* plays a crucial role in vascular development and endothelial cell function, which are integral to the health and function of adipose tissue (47). *SAMM50* is involved in beige adipocyte thermogenesis and energy balance (48). Shared genetic architecture between the peripheral fat and lower-body fat axes, including genes like *RSPO3*, *COBLL1*, and *DNAH10OS*, points to overlapping mechanisms. Additionally, genes involved in adipogenesis, lipid metabolism, and insulin signaling emerged as key drivers of these axes. Tissue-specific eQTLs in skeletal muscle and adipose tissue further underscore the role of regulatory mechanisms in shaping these phenotypes.

### Clinical Implications and Future Directions

Our study provides novel insights into the heterogeneity of obesity by leveraging MRI-derived phenotypes to define distinct obesity axes. Unlike traditional measures such as BMI (2), our approach offers a more granular assessment of body composition and its genetic determinants, revealing that individuals with similar BMIs can present vastly different patterns of fat distribution and metabolic risk. We show that these axes have distinct genetic backgrounds, with no evidence of sex-specific associations, suggesting that genetic influences on fat distribution and muscle volume are largely shared between men and women. Although many of the genetic markers we identified have been previously implicated in adiposity, our findings, such as the associations linking *RSPO3* and *COBLL1* to the lower-body fat axis and unique loci for the muscle-dominant axis, underscore the complexity of obesity and suggest that the underlying biological mechanisms differ across these axes.

Although these findings are not yet directly applicable in clinical practice, they lay the groundwork potentially for future precision medicine approaches. As imaging technologies become more accessible, MRI-derived obesity classifications may eventually allow for targeted interventions that address specific patterns of fat distribution and muscle composition. Furthermore, our study highlights the potential value of risk stratification beyond BMI, because even individuals classified as living with obesity by conventional standards may have different disease trajectories. Also, understanding the genetic architecture of these obesity axes may guide therapeutic research, particularly in developing treatments that modulate fat storage patterns or muscle composition to mitigate metabolic risk. Future work should focus on replicating these findings in more diverse populations and on investigating whether these obesity axes predict incident disease risk over time, ultimately guiding the development of tailored therapeutic strategies. How newer weight loss therapies influence body compositional changes and future outcome risks in these different obesity phenotypes will also be of interest.

### Strengths and Limitations

This study's strengths include its large sample size and the use of advanced MRI to define obesity axes. However, limitations include the restriction of analyses to individuals of White British ancestry, which may affect the generalizability of the findings to other populations. Future studies should replicate these findings in more diverse cohorts. Additionally, although MR provided causal insights, potential residual confounding or pleiotropic effects cannot be completely ruled out.

### Conclusion

This study highlights the complexity and heterogeneity of obesity by identifying distinct axes with unique genetic, metabolic, and disease risk profiles. The potential to extend beyond BMI and integrate advanced imaging with multiomic data provides a nuanced understanding of obesity. These findings pave the way for more personalized approaches to obesity treatment and prevention, tailored to an individual's genetic, metabolic, and fat distribution profile.

**Acknowledgments.** This research was conducted using the UK Biobank resource under application 44584. The authors also acknowledge the participants and investigators of the FinnGen study.

**Funding.** H.Y. is supported by Diabetes UK (grant 23/0006598). C.S.O. and H.Y. are supported by Calico Life Sciences, LLC.

**Duality of Interest.** N.S. has received grants and personal fees from AstraZeneca, Boehringer Ingelheim, and Novartis; a grant from Roche Diagnostics; and personal fees from Abbott Laboratories, Afimmune, Amgen, Eli Lilly, Hanmi Pharmaceuticals, Merck Sharp & Dohme, Novo Nordisk, Pfizer, and Sanofi, outside the submitted work. M.C. and E.P.S. are employees of

Calico Life Sciences, LLC. No other potential conflicts of interest relevant to this article were reported.

**Author Contributions.** C.S.O. and A.N. analyzed the data. M.T., B.W., J.D.B., E.L.T., and M.C. provided all the MRI-derived IDPs. E.P.S. and N.S. contributed to the reviewing, editing, and approving the manuscript. M.C. performed the GWAS. All authors contributed to reviewing, editing, and approving the manuscript. H.Y. designed the study and wrote the manuscript. H.Y. is the guarantor of this work and, as such, had full access to all the data in the study and takes responsibility for the integrity of the data and the accuracy of the data analysis.

## References

1. Elmaleh-Sachs A, Schwartz JL, Bramante CT, Nicklas JM, Gudzune KA, Jay M. Obesity management in adults: a review. JAMA 2023;330:2000–2015
2. Abraham A, Yaghootkar H. Identifying obesity subtypes: a review of studies utilising clinical biomarkers and genetic data. Diabet Med 2023;40:e15226
3. Bray GA. Medical consequences of obesity. J Clin Endocrinol Metab 2004; 89:2583–2589
4. Perdomo CM, Cohen RV, Sumithran P, Clément K, Frühbeck G. Contemporary medical, device, and surgical therapies for obesity in adults. Lancet 2023;401: 1116–1130
5. Pillon NJ, Loos RJF, Marshall SM, Zierath JR. Metabolic consequences of obesity and type 2 diabetes: balancing genes and environment for personalized care. Cell 2021;184:1530–1544
6. Zhou Z, Macpherson J, Gray SR, et al. Are people with metabolically healthy obesity really healthy? A prospective cohort study of 381,363 UK Biobank participants. Diabetologia 2021;64:1963–1972
7. Ahima RS, Lazar MA. Physiology. The health risk of obesity-better metrics imperative. Science 2013;341:856–858
8. Bodaghi A, Fattahi N, Ramazani A. Biomarkers: promising and valuable tools towards diagnosis, prognosis and treatment of Covid-19 and other diseases. Heliyon 2023;9:e13323
9. Yaghootkar H, Whitcher B, Bell JD, Thomas EL. Ethnic differences in adiposity and diabetes risk – insights from genetic studies. J Intern Med 2020; 288:271–283
10. Littlejohns TJ, Holliday J, Gibson LM, et al. The UK Biobank imaging enhancement of 100,000 participants: rationale, data collection, management and future directions. Nat Commun 2020;11:2624
11. Basty N, Liu Y, Cule M, Thomas EL, Bell JD, Whitcher B. Automated measurement of pancreatic fat and iron concentration using multi-echo and T1-weighted MRI data. 17th International Symposium on Biomedical Imaging, Iowa City, IA, 2020, IEEE, p. 345–348
12. Liu Y, Basty N, Whitcher B, et al. Genetic architecture of 11 organ traits derived from abdominal MRI using deep learning. Elife 2021;10:e65554
13. Whitcher B, Thanaj M, Cule M, et al. Precision MRI phenotyping enables detection of small changes in body composition for longitudinal cohorts. Sci Rep 2022;12:3748
14. Thanaj M, Basty N, Whitcher B, et al. Precision MRI phenotyping of muscle volume and quality at a population scale. Front Physiol 2024;15:1288657
15. Bydder M, Ghodrati V, Gao Y, Robson MD, Yang Y, Hu P. Constraints in estimating the proton density fat fraction. Magn Reson Imaging 2020;66:1–8
16. Mbatchou J, Barnard L, Backman J, et al. Computationally efficient whole-genome regression for quantitative and binary traits. Nat Genet 2021;53: 1097–1103
17. Bycroft C, Freeman C, Petkova D, et al. The UK Biobank resource with deep phenotyping and genomic data. Nature 2018;562:203–209
18. Watanabe K, Taskesen E, van Bochoven A, Posthuma D. Functional mapping and annotation of genetic associations with FUMA. Nat Commun 2017;8:1826
19. GTEx Consortium. The GTEx Consortium atlas of genetic regulatory effects across human tissues. Science 2020;369:1318–1330
20. Thomas PD, Ebert D, Muruganujan A, Mushayahama T, Albou L-P, Mi H. PANTHER: making genome-scale phylogenetics accessible to all. Protein Sci 2022;31:8–22
21. Bulik-Sullivan B, Finucane HK, Anttila V, et al.; Genetic Consortium for Anorexia Nervosa of the Wellcome Trust Case Control Consortium 3. An atlas of genetic correlations across human diseases and traits. Nat Genet 2015;47:1236–1241
22. Burgess S, Thompson SG. Interpreting findings from Mendelian randomization using the MR-Egger method. Eur J Epidemiol 2017;32:377–389
23. Magkos F, Sørensen TIA, Raubenheimer D, et al. On the pathogenesis of obesity: causal models and missing pieces of the puzzle. Nat Metab 2024;6: 1856–1865
24. Martin S, Tyrrell J, Thomas EL, et al.; INVENT Consortium. Correction: disease consequences of higher adiposity uncoupled from its adverse metabolic effects using Mendelian randomisation. Elife 2022;11:e80233
25. Pivonello R, De Martino MC, De Leo M, Simeoli C, Colao A. Cushing's disease: the burden of illness. Endocrine 2017;56:10–18
26. Kim G, Lee S-E, Jun JE, et al. Increase in relative skeletal muscle mass over time and its inverse association with metabolic syndrome development: a 7-year retrospective cohort study. Cardiovasc Diabetol 2018;17:23
27. Wang Z, Wu M, Shao X, Yang Q. Muscle quality index is associated with depression among non-elderly US adults. BMC Psychiatry 2024;24:672
28. Yaghootkar H, Scott RA, White CC, et al. Genetic evidence for a normal-weight "metabolically obese" phenotype linking insulin resistance, hypertension, coronary artery disease, and type 2 diabetes. Diabetes 2014;63:4369–4377
29. Yaghootkar H, Lotta LA, Tyrrell J, et al. Genetic evidence for a link between favorable adiposity and lower risk of type 2 diabetes, hypertension, and heart disease. Diabetes 2016;65:2448–2460
30. Lotta LA, Gulati P, Day FR, et al.; Cambridge FPLD1 Consortium. Integrative genomic analysis implicates limited peripheral adipose storage capacity in the pathogenesis of human insulin resistance. Nat Genet 2017;49:17–26
31. Ji Y, Yiorkas AM, Frau F, et al. Genome-wide and abdominal MRI data provide evidence that a genetically determined favorable adiposity phenotype is characterized by lower ectopic liver fat and lower risk of type 2 diabetes, heart disease, and hypertension. Diabetes 2019;68:207–219
32. Abraham A, Cule M, Thanaj M, et al. Genetic evidence for distinct biological mechanisms that link adiposity to type 2 diabetes: toward precision medicine. Diabetes 2024;73:1012–1025
33. Martin S, Cule M, Basty N, et al. Genetic evidence for different adiposity phenotypes and their opposing influences on ectopic fat and risk of cardiometabolic disease. Diabetes 2021;70:1843–1856
34. Ahmed A, Justo S, Yaghootkar H. Genetic scores associated with favourable and unfavourable adiposity have consistent effect on metabolic profile and disease risk across diverse ethnic groups. Diabet Med 2023;40:e15213
35. Endo Y, Groom L, Wang SM, et al. Two zebrafish cacna1s loss-of-function variants provide models of mild and severe CACNA1S-related myopathy. Hum Mol Genet 2024;33:254–269
36. Fuentes MA, Piper HN, He B. Dlg1 regulates subcellular distribution of non-muscle myosin II during Drosophila germband extension. bioRxiv. 29 August 2022 [preprint]. DOI: 10.1101/2022.08.29.505652
37. Chen T-C, Kuo T, Dandan M, et al. The role of striated muscle Pik3r1 in glucose and protein metabolism following chronic glucocorticoid exposure. J Biol Chem 2021;296:100395
38. Hayashi S, Manabe I, Suzuki Y, Relaix F, Oishi Y. Klf5 regulates muscle differentiation by directly targeting muscle-specific genes in cooperation with MyoD in mice. Elife 2016;5:e17462
39. Baldelli S, Ciccarone F, Limongi D, Checconi P, Palamara AT, Ciriolo MR. Glutathione and nitric oxide: key team players in use and disuse of skeletal muscle. Nutrients 2019;11:2318
40. Carnio S, LoVerso F, Baraibar MA, et al. Autophagy impairment in muscle induces neuromuscular junction degeneration and precocious aging. Cell Rep 2014;8:1509–1521

41. Saran S, Tran DDH, Klebba-Färber S, et al. THOC5, a member of the mRNA export complex, contributes to processing of a subset of wingless/integrated (Wnt) target mRNAs and integrity of the gut epithelial barrier. BMC Cell Biol 2013;14:51–14
42. Glunk V, Laber S, Sinnott-Armstrong N, et al. A non-coding variant linked to metabolic obesity with normal weight affects actin remodelling in subcutaneous adipocytes. Nat Metab 2023;5:861–879
43. Loh NY, Minchin JEN, Pinnick KE, et al. RSPO3 impacts body fat distribution and regulates adipose cell biology in vitro. Nat Commun 2020;11:2797
44. Chen G, Zhou G, Zhai L, et al. SHMT2 reduces fatty liver but is necessary for liver inflammation and fibrosis in mice. Commun Biol 2024;7:173
45. Cox N, Crozet L, Holtman IR, et al. Diet-regulated production of PDGFcc by macrophages controls energy storage. Science 2021;373 eabe9383
46. Pellegrinelli V, Rodriguez-Cuenca S, Rouault C, et al. Dysregulation of macrophage PEPD in obesity determines adipose tissue fibro-inflammation and insulin resistance. Nat Metab 2022;4:476–494
47. Lee M, Betz C, Yin J, et al. Control of dynamic cell behaviors during angiogenesis and anastomosis by Rasip1. Development 2021;148:dev197509
48. Park S-J, Shon D-H, Kim J-H, Ryu Y-H, Ko Y. SAMM50 regulates thermogenesis of beige adipocytes differentiated from human adipose-derived stem cells by balancing mitochondrial dynamics. Int J Mol Sci 2022;23:6764